



RESEARCH ARTICLE

**MXENE 2D  $Ti_3C_2T_x$  PRODUCTION AND SPIN-ORBIT EFFECT (SOI) OF  $Ti_3C_2(OH)_2$  IN THE ELECTRONIC STRUCTURE**

**Mesut Ramazan EKİCİ<sup>1,\*</sup>, Hüseyin Yasin UZUNOK<sup>2</sup>, Emrah BULUT<sup>3,4</sup>, Hüseyin Murat TÛTÛNCÛ<sup>5</sup>, Ahmet ATASOY<sup>6</sup>**

<sup>1</sup> Sakarya University, Metallurgical and Materials Engineering, Sakarya, Türkiye.

[mekici@sakarya.edu.tr](mailto:mekici@sakarya.edu.tr) - [0000-0002-3024-2567](https://orcid.org/0000-0002-3024-2567)

<sup>2</sup> Sakarya University, Faculty of Sciences, Physics, Sakarya, Türkiye

[hyuzunok@sakarya.edu.tr](mailto:hyuzunok@sakarya.edu.tr) - [0000-0002-2130-1748](https://orcid.org/0000-0002-2130-1748)

<sup>3</sup> Sakarya University, Faculty of Sciences, Chemistry, Sakarya, Türkiye

<sup>4</sup> Sakarya University Research Development & Application Center-SARGEM, Sakarya, Türkiye

[ebulut@sakarya.edu.tr](mailto:ebulut@sakarya.edu.tr) - [0000-0002-7623-8088](https://orcid.org/0000-0002-7623-8088)

<sup>5</sup> Sakarya University, Faculty of Sciences, Physics, Sakarya, Türkiye

[tutuncu@sakarya.edu.tr](mailto:tutuncu@sakarya.edu.tr) - [0000-0003-1979-1626](https://orcid.org/0000-0003-1979-1626)

<sup>6</sup> Sakarya University of Applied Sciences, Faculty of Technology, Metallurgical and Materials Engineering, Sakarya, Türkiye

[atasoy@sakarya.edu.tr](mailto:atasoy@sakarya.edu.tr) - [0000-0003-1564-8793](https://orcid.org/0000-0003-1564-8793)

**Abstract**

Research on new-generation materials to meet the energy needs has begun to attract attention. Recently, energy storage in materials has become the most researched area. As a result of the reaction of the MAX phase 312  $Ti_3SiC_2$  powder with hydrofluoric acid, a new 2D nanosized layered powder called MXene, similar to graphene, was obtained. MXenes, which have been studied in various sectors, especially energy, have attracted the attention of researchers owing to their multilayered structures. When  $Ti_3SiC_2$  powder was treated with hydrofluoric acid (HF), an accordion-like two-dimensional  $Ti_3C_2T_x$  MXene structure was formed. In MXenes, surface coatings such as  $-O$ ,  $-OH$ , and  $-F$  groups, which determine and affect various aspects of 2D materials, such as conductivity, constitute the application area. In this study,  $Ti_3C_2(OH)_2-O$  and/or  $-OH$  surface terminations were examined using density functional theory (DFT) with the effect of the hydrofluoric acid etching time. Quantum Espresso program was used for DFT calculation. X-ray diffraction (XRD) and scanning electron microscopy (SEM and FESEM) were used to examine the MXene-phase  $Ti_3C_2T_x$  powder and first-principles calculations were performed. The structural and electronic properties of MAX and MXene compounds were determined. The spin-orbit effect (SOI) was examined in the electronic structure of MXene. The total and partial densities of states (DOS) with and without spin orbit were calculated.

**Keywords**

MXene,  
 $Ti_3SiC_2$ ,  
Spin-orbit,  
DFT,  
2D Material

**Time Scale of Article**

Received : 16 December 2023  
Accepted : 20 July 2024  
Online date : 30 September 2024

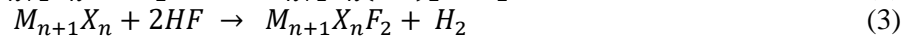
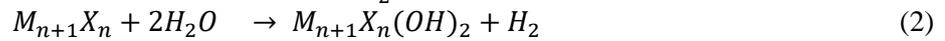
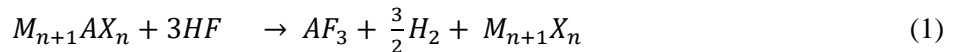
\*Corresponding Author: [mekici@sakarya.edu.tr](mailto:mekici@sakarya.edu.tr)

## 1. INTRODUCTION

In 2011, a team led by Drexel University's Yury Gogotsi and Michel W. Barsoum discovered that selective etching of the MAX phase could yield a novel 2-dimensional transition metal carbide phase. The removal of the A layer from the MAX phase (MX) and its similarity to graphene (ene) resulted in the formation of MXene, a novel 2-dimensional carbide/nitride phase transition metal. Selective etching of Al was achieved by immersing Al-containing MAX phases in hydrofluoric (HF) acid, resulting in two-dimensional (2D) materials called MXenes [1], [2], [11]–[14], [3]–[10]. MXenes, the most researched materials, have been used in lithium-ion batteries, electrochemical capacitors, and fuel cells. Furthermore, the rich chemistry of MXenes, along with their ability to modify the composition, even along a single atomic plane, provide intriguing qualities for "temporary" battery designs, where the electrode can operate depending on the material used [15]–[17]. By integrating Li-ions into MXene layers, MXene appears to be a good candidate for electrode materials for Lithium-ion batteries (LIBs) and supercapacitors. MXene reveals that it has the potential to be an excellent high-capacity anode material [15], [18]–[21].

MAX phases are carbides or nitrides with three layers, and their theoretical formula is  $M_{n+1}AX_n$  ( $n = 1, 2, 3$ ). Where M is an early transition metal, A is a group A element, and X is either carbon or nitrogen. MAX Phases have good electrical and thermal conductivities (e.g., metals), easy machinability, flexibility, good thermal shock resistance (e.g., ceramics), high strength, toughness, high temperature, and thermal and chemical stability. It is a fantastic material that combines the qualities of metals and ceramics [22]–[25]. MXene is a two-dimensional (2D) transition metal carbide and nitride nanomaterial with the chemical formula  $M_{n+1}X_nT_x$ .  $T_x$  represents the surface group.  $T_x$  surface terminations include fluorine (–F), hydroxyl (–OH), and oxygen (–O) [26]–[32].

MXenes are used in a wide range of applications. Field effect transistors [7], [33]–[36], biomaterial [6], [37], [38], suitable substrate for paints [13], [35], electromagnetic interface screensavers [32], [39], electrodes [7], [8], [26], [40], [41], catalyst [28], [32], [42], optical [32], [43], batteries [26], [44]–[47], composites [26], [32], reactor [30], [48], [49], sensor (gas sensor, biosensor, pressure sensor, strain sensor) [6], [8], [26], [50]–[52], water treatment [6], [8], [14], [26], [50], super capacitor [28], [32], transparent conductors [6], [32] is used. Finishing processes for MXene production (–F, –O, and/or –OH);



The supernatant ( $AF_3$ ) and  $\frac{3}{2}H_2$  were removed from the MAX phase when combined with hydrofluoric acid (Equation 1) to produce  $M_{n+1}X_n$ . MXene is produce when the  $M_{n+1}X_n$  phase combines with either water (Equation 2) or hydrofluoric acid (Equation 3). The surface termination in Equation 2 is oxygen (–O) and/or hydroxyl (–OH). The surface termination in Equation 3 is fluorine (–F) [34], [53]. The surface-finishing processes of  $Ti_3SiC_2$  are presented in Tables 1 [29], [50], [54], [55]. The  $T_x$  component of  $Ti_3C_2T_x$  formed as a result of these reactions can be –F ( $Ti_3C_2F_2$ ), –O ( $Ti_3C_2O_2$ ), or –OH ( $Ti_3C_2(OH)_2$ ) [56]–[60].

**Table 1.** Different surface finishing processes of Ti<sub>3</sub>SiC<sub>2</sub> [61]–[63].

Step 1	Step 2
Ti <sub>3</sub> SiC <sub>2</sub> + 3HF = Ti <sub>3</sub> C <sub>2</sub> + SiF <sub>3</sub> + 3/2H <sub>2</sub>	Ti <sub>3</sub> C <sub>2</sub> + 2HF = Ti <sub>3</sub> C <sub>2</sub> F <sub>2</sub> + H <sub>2</sub>
	Ti <sub>3</sub> C <sub>2</sub> + O <sub>2</sub> = Ti <sub>3</sub> C <sub>2</sub> O <sub>2</sub>
	Ti <sub>3</sub> C <sub>2</sub> + 2H <sub>2</sub> O = Ti <sub>3</sub> C <sub>2</sub> (OH) <sub>2</sub> + H <sub>2</sub>

Owing to their ceramic properties, MXenes are chemically and mechanically stable. MXenes have various shapes and sizes, including single- and multilayered structures. It can be made as a complex material from a mix of light and heavy transition metals, allowing the number of valence electrons and relativistic spin-orbit coupling to be adjusted. This improved the electronic performance and mechanical stability of the devices. Thus, the thickness of the MXene layer can be changed. MXene surfaces can be functionalized with various chemical groups, allowing surface state engineering. Some MXenes exhibit massless Dirac dispersions in bands close to the Fermi level. This broadens the scope of dirac-based physics and its applications. These characteristics distinguish MXene from other compounds. The electrical properties of MXenes, such as conductivity, band gap, and operational function, are determined by their terminal groups and X-elements, which determine whether they are metallic or semiconducting [32], [64].

MAX-phase bonding generally involves metallic, covalent, and ionic interactions. A strong M - X link is covalent, metallic, and ionic, whereas an M - A bond is metallic. The weak ionic-covalent connections between M and X are too strong to break easily. They were separated into three groups: 2 (211), 3 (312), and 4 (413), corresponding to the M layer, depending on the number of M layers separating the A layers. MAX phases have structures that are composed of several metals. Ionic M-A bonds are connected by weak covalent M-X bonds. Consequently, the atoms of element A are far more reactive than those of elements M and X. The most basic principle for accessing MXenes is selective etching; using an acidic fluoride solution, removing A element layers without damaging the M-X bonds is possible. MAX phases have high binding strength owing to their metallic, ionic, and covalent bonds. Because the metallic link between Ti and Si is weaker than the covalent bond between Ti and C, HF etching selectively eliminates the Si layer from Ti<sub>3</sub>SiC<sub>2</sub>. The Ti<sub>3</sub>C<sub>2</sub> layers were joined with Si atomic layers, which acted as mirror planes in Ti<sub>3</sub>SiC<sub>2</sub>. Si-Ti bonds are weak, but Ti-C bonds are significantly more durable. Ti<sub>3</sub>SiC<sub>2</sub> exhibits exceptional mechanical characteristics and chemical stability at high temperatures. The structure combines metallic and ceramic characteristics with layered crystalline metallic (M-A) and covalent (M-X) links. The MAX phases are good thermal and electrical conductors. M-X bonds are among the most powerful in nature [14], [15], [42], [52].

The addition of metal ions or organic molecules and the combination of inorganic particles and MXene layers control and optimize the MXene properties [50]. MXene (Ti<sub>3</sub>C<sub>2</sub>T<sub>x</sub>) layers can be intercalated in various ways owing to the weak bonds between the M<sub>n+1</sub>X<sub>n</sub> layers [6], [34]. The number of hydrogen bonds and/or the bonds between the Van der Waals Ti<sub>3</sub>C<sub>2</sub>T<sub>x</sub> layers decreased after joining dimethyl sulfoxide (DMSO) [65], [66]. Inorganic molecules (metal cations and water) can easily combine with MXene, widening the space between layers [6], [34], [67]. MXenes with these molecules, followed by mechanical vibration or sonication in water, form colloidal monolayers and multilayer MXenes [26]. After intercalation, single or few layers of Ti<sub>3</sub>C<sub>2</sub>T<sub>x</sub> were split into layers (nanosheets/flakes) by direct handshaking or mechanical vibration (bath sonication stage), and a stable colloidal solution was formed [34], [65], [68], [69].

## 2. EXPERIMENTAL PROCEDURES

MAX phase powder-mixing ratio was used for MXene synthesis. The MAX-phase powder was mixed with 10 mL of acid solution [2], [55], [61]–[63], [70], [71]. In the experiments, Teflon Magnetic Fish (PTFE) and plastic beakers did not react. The mixture was stirred using a magnetic stirrer with Teflon magnetic fish in a plastic bottle [45], [72].

MAX-phase  $\text{Ti}_3\text{SiC}_2$  powder with a 200-mesh size and 98 per cent purity (2% TiC) was obtained from Forsman Scientific (Beijing) Co., Ltd. For 1 g of  $\text{Ti}_3\text{SiC}_2$  powder, 10 ml of acid solution was used. Acid (50 per cent) was used as an acid. The powder was slowly added to the solution owing to the exothermic reaction. The resultant solution was mixed for 8 h and 32 h in a fume hood with a magnetic stirrer set at 750 rpm. Table 2 lists the codes for the sample samples prepared based on the mixing time.

**Table 2.** Mixing times of  $\text{Ti}_3\text{SiC}_2$  and  $\text{Ti}_3\text{C}_2\text{T}_x$  powders.

Sample	Acid/Solution	Hours	Code
Sample 1	-	-	$\text{Ti}_3\text{SiC}_2$
Sample 2	HF	8	HF-8
Sample 3	HF	32	HF-32
Sample 4	HF+HF	8+8	HF-HF-8
Sample 5	HF+HF	32+32	HF-HF-32
Sample 6	HF+HF+DMSO	8+8+18	HF-HF-DMSO-8
Sample 7	HF+HF+DMSO	32+32+18	HF-HF-DMSO-32

The PTFE was placed in a beaker to mix the plastic. The powders obtained after HF treatment were subjected to HF (HF-HF) treatment. Centrifugation with deionized water was rounded off in MXene manufacturing to neutralize the acidic environment caused by the reaction of MAX-phase particles with acid. A link exists between the pH level and the mixing process. The pH of the supernatant determines the time required for centrifugation. The pH value of the supernatant solution is 4–6 [6], [8], pH value is between 5–6 [18], [29], [34], [42], [65], [69], pH value is between 6–7 [15], [35], [46]. In some studies, the pH was considered sufficient to achieve neutrality [9], [36]. More centrifugation was required to achieve an appropriate pH shift, which was directly affected by centrifugation the HF reactions. Numerous elements influence the MXene production. Many factors alter the physical and chemical properties of MXenes, which, in turn, affect their quality. The solution ratio, mixing duration, acid variety, organic chemicals, temperature, pressure, and surface finishing are the most critical variables. One of the most important factors that determines the quality and yield of MXenes is the solution ratio. The chemical stability of MXene increases as the number of layers increases.  $\text{Ti}_3\text{C}_2\text{T}_x$  has 50 per cent HF and 100 per cent efficiency, whereas  $\text{Ti}_2\text{CT}_x$  has 60 per cent efficiency with only 10% HF [20]. For MXenes, the mixing time is effective for surface finishing. Increasing the -O terminations while lowering the HF concentration lowers the -F terminations [14]. Some XRD peaks may vanish, whereas others may return because of mixing time. The processing time increased with HF to attain higher angle values. This indicates that when the processing time with HF increases, the d-distances of the planes decrease [73]. The increased mixing time reduces the particle size, resulting in a faster transition from the MAX phase to the MXene phase. Although there was no notable change in the mixing after a short period, the MXene phase was created with alterations in the MAX phase structure over long mixing times [52]. The mixing time decreased with an increase in the temperature of the mixture. Temperature and time showed an inverse relationship. For example, mixing for 48 h at 35 °C is comparable to mixing for 24 h at 60 °C [1].

The Al layers were replaced with surface terminal groups presumed to be -O, -OH, and/or -F during the chemical etching of the MAX phases to form the MXene phases. According to DFT calculations, surface terminations can directly or indirectly modify the electronic characteristics of MXenes from

semiconductors with small bandgaps to semiconductors with wide bandgaps. Termination causes variations in the bandgap. The capacity of oxygen-terminated MXenes was calculated to be higher than those of hydroxyl- and F-terminated MXenes [14]. Centrifugation is necessary for manufacturing MXenes. After combining with acid, the centrifugation speed and time helped the solution to become neutral (pH 5-6). Although the centrifuge speed varied, it was typically set to 3500 rpm [34]–[36], [69]. The fluid and powder were mixed using a magnetic stirrer and transferred to a centrifuge tube. Centrifugation was performed at 3500 rpm for 5 min [62], [63]. pH measurements were performed in the supernatant of the centrifuge tube before it was emptied. The pH meter was washed with distilled water for each particle size. Centrifugation was performed for 5 min until the pH level reached 5-6. After centrifugation, the pH of the MXene powder increased logarithmically. There was a proportionate variance between the time spent mixing with HF and the time spent centrifuging (Fig. 1).

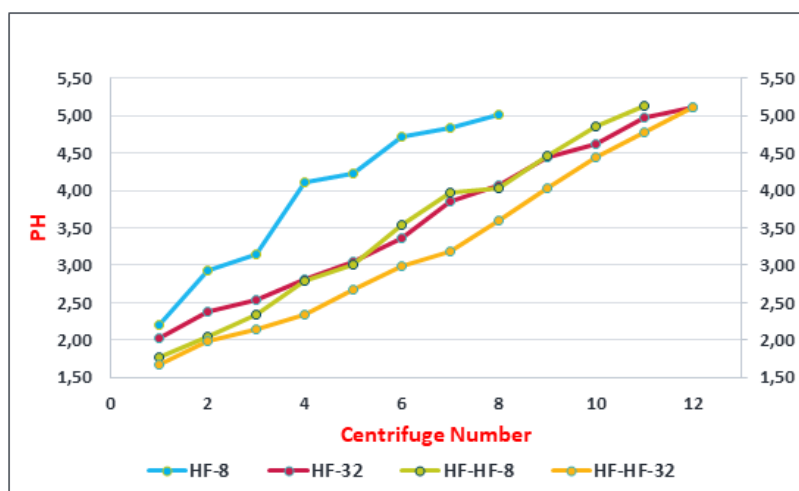


**Figure 1.** pH change in the powder produced with hydrofluoric acid (HF) by centrifugation.

Filtering removes the MXene particle solution from deionized water. A mud (clay)-like structure was formed after filtration [33], [36], [42], [52], [74], [75]. After mixing, the supernatant was filtered using a filter. The liquid waste portion of the supernatant was emptied into other containers. Following centrifugation of the solution obtained by mixing it with HF, the supernatant-colored turquoise was obtained. The amount of silicon in the supernatant was determined by chemical analysis. The layers generated by breaking the Van der Waals bonds between the layers were split into further layers by sonication after intercalation with an organic solvent (e.g. dimethyl sulfoxide). This enables mechanical vibration or hand shaking to open layers [26], [34], [66].

Ethyl alcohol (40 mL) was poured into a glass beaker. The sonicator was sonicated for 6 hours in 1-hour chunks. Each hour, four cycles were completed at 15-minute intervals, with sonication creating 5-second pulses.

Each cycle included a 5-minute rest time after the warm-ups. The mixture was submerged in an ultrasonic bath for one hour. For one gramme of MXene particles, 500 ml of deionized water was placed in an ultrasonic bath at a frequency of 37 kHz. The MXene particles broke and were delaminated in both the ultrasonic treatments. The layered MXene structures were mixed with DMSO for 18 h at room temperature. To 1 g of MXene, 20 ml DMSO was used [42], [52], [64], [65], [76]. The mixture was centrifuged at 4000 rpm for 10 min to separate the DMSO from the mixture. This phenomenon is known as delamination [14], [15], [21], [67]. After centrifugation, the mixture was filtered through a 200 nm porous membrane filter. It was then dried in a vacuum oven at 70 °C for 24 h [15], [34], [35], [67], [77]. Figure 2 shows the MXene phase.

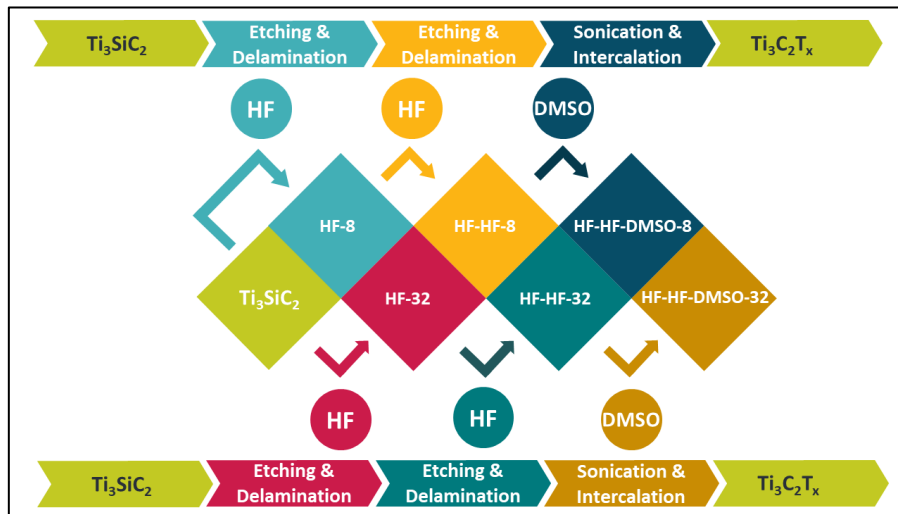


Figure 2. MXene production steps

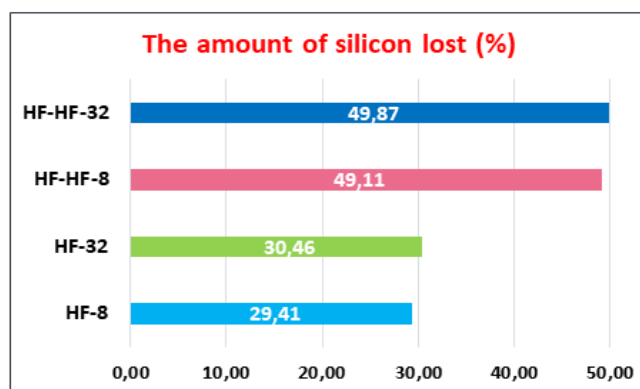
After centrifugation and filtration, a moist, clay-like texture was observed. The powders were dried in a vacuum oven for 24 hours at a temperature of 70-80 °C [34], [65], [66], [78]. To filter the clay (mud) from the powder and separate it from the liquid, vacuum filtration was conducted for approximately one hour. Subsequently, it was dried in a vacuum oven at 70 °C for 24 h. Table 3 lists the chemical methods used for the powders.

Table 3. Processes used in the manufacture of MAX Phase Ti3SiC2 powders using MXene.

Code	Etching	Delamination	Sonication	Intercalation
Ti3SiC2	-	-	-	-
HF-8	+	+	-	-
HF-32	+	+	-	-
HF-HF-8	++	++	+	-
HF-HF-32	++	++	+	-
HF-HF-DMSO-8	++	++	+	+
HF-HF-DMSO-32	++	++	+	+

There are losses in the powder production when MXene is produced from the MAX phase. One gram of Ti3SiC2 contained 0.140852 g silicon. The loss of silicon or the amount of silicon in the supernatant was determined using EDX analysis. The amount of silicon in the supernatant was measured.

The silicon ratio in the supernatant solution is measured in ppm using the Spectro Arcos FHE16 model Inductively Coupled Plasma (ICP)-Optical Emission Spectrometer (OES) equipment (Figure 3). First, reference silicon standard solutions were prepared. The silicon content in the model (supernatant) was determined by comparing the ratio of the sample to the standard solution (Figure 3). Because of the reaction with HF, the MAX phase powders removed Si from the atmosphere; however, some Si remained in the powder.



**Figure 3.** MXene synthesis from the MAX phase resulted in a percentage weight loss of silicon in  $Ti_3C_2T_x$  powder.

Because of the fluorine ratio in HF etching, a lower HF acid ratio results in more oxygen. In the etching process with 10% HF, more oxygen and less fluorine are observed than in the etching process with 50% HF. The most important factor in surface finishing is acidity [26], [42]. Because the etching process involves an exothermic reaction, vigilance should be exercised and the reaction vessel should be thoroughly ventilated [9], [50]. Owing to the risk associated with HF, other acids can be used as alternative corrosives. The MXene layer developed flaws because of HF's high etching ability of HF [32], [50]. The functional groups in the generated MXenes impart hydrophilicity to surface terminations [68].

## 2.1. Theoretical Calculations

This study was carried out using the Quantum-Espresso [79], [80] simulation package based on density functional theory. The electron–electron interaction was processed by GGA using the existing Perdew-Burke-Ernzerhof [81]. Coulomb interactions between valence electrons and ionic nuclei were described using full and scalar relativistic ultrasoft pseudopotentials to determine the effects of spin–orbit interaction (SOI) on the physical properties of all compounds studied. The maximum plane-wave cutoff energy was set at 60 Ry, whereas the electronic charge density was expanded on a basic cutoff basis up to 600 Ry. Self-consistent solutions of the Kohn-Sham equations were determined using Monkhorst-Pack special k-points [82] within the Brillouin zone (BZ). While the total energy calculations for all compounds examined were performed on a  $(12 \times 12 \times 12)$  k-point network, this network was increased to  $(24 \times 24 \times 24)$  for electronic measurements.

## 2.2. Structural and Electronic Properties

The studied  $Ti_3SiC_2$  and its MXene-phase  $Ti_3C_2(OH)_2$  compounds crystallized in a hexagonal  $p63/mmc$  (Wyckoff number of 194) structure, as shown in Figure 4. As shown in Figure 4 (a), the polyhedral was formed into an octahedral pyramid, with the Ti atom placed at its center. Some of the C atoms from the neighboring unit cells are also shown to better understand these polyhedra and bonds. Crossing Ti atoms formed six bonds with neighboring C and Si atoms. For  $Ti_3C_2(OH)_2$ , polyhedra occur between Ti and C atoms and have a triangular pyramid shape. The coordinates of the Ti atoms were 2a (0.00,0.00,0.00), 4f ( $1/3, 2/3, z_{Ti}$ ), Si atoms were 2b (0.00, 0.00,  $1/4$ ), C atoms were 4f ( $1/3, 2/3, z_C$ ), O atoms were 4e (0.00, 0.00,  $z_O$ ), and H atoms were 4e (0.00, 0.00,  $z_H$ ). The lattice parameters of  $Ti_3SiC_2$  were obtained from a previous experimental study [82]. Structural relaxation calculations were performed for  $Ti_3C_2(OH)_2$ ; structural relaxation calculations were performed, and the obtained values for its lattice parameters were  $a = 3.21 \text{ \AA}$ , and  $c = 22.38 \text{ \AA}$ . The inner parameters for atoms are  $z_{Ti} = 0.6122$ ,  $z_C = 0.5746$ ,  $z_O = 0.4133$ , and  $z_H = 0.2151$  for  $Ti_3C_2(OH)_2$ . The C atoms formed three bonds with O atoms and one bond with a Ti atom, with a total of four bonds. The bond length between Ti-C in  $Ti_3C_2(OH)_2$  is  $2.088 \text{ \AA}$ , which is longer than the corresponding value of  $2.081 \text{ \AA}$  in  $Ti_3SiC_2$ . Because the electronegativities of the atoms

are different in both compounds, we can say that the bonding in the studied compounds is an admixture of covalent, ionic, and metallic behaviors.

The calculated electronic band structure of the MAX Phase  $Ti_3SiC_2$  compound is presented in Figure 5 along with the high-symmetry directions of the Brillouin region of the hexagonal system. The Fermi level was set to 0 eV and is indicated by dashed blue lines with significantly high symmetry points. Because several bands cross the Fermi level along all symmetry directions, it was concluded that this compound exhibits a metallic behavior. These results agree with those of previous studies of this compound [83]. While the red dashed lines are obtained by including the SOI, the dashed black lines represent the electronic structure without the SOI. As shown in Figure 5., the SOI had almost no effect on the electronic band structure of the compound.

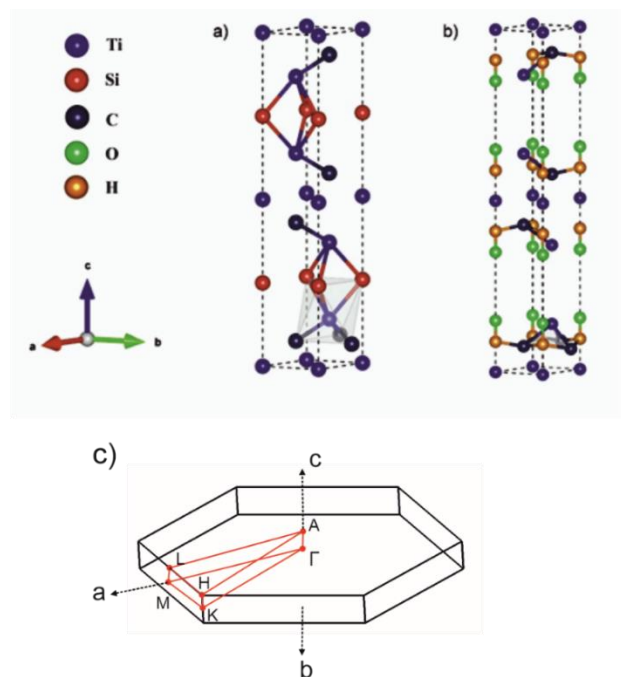


**Figure 4.** Crystal structures of a)  $Ti_3SiC_2$ , b)  $Ti_3C_2(OH)_2$  compounds, and (c) high-symmetry points of the hexagonal structure

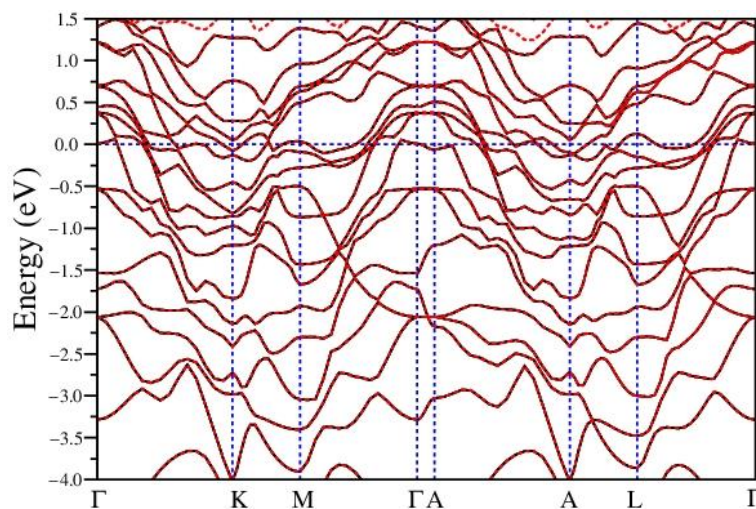


**Figure 5.** Electronic structures of  $Ti_3SiC_2$  with (red dashed lines) and without (solid black lines) spin-orbit interactions

However, the electronic structure of  $\text{Ti}_3\text{C}_2(\text{OH})_2$  exhibits features different from those of its MAX phase, as shown in Figure 6. Splitting due to the SOI increases the electronic bands that cross the  $E_F$  and enhances the free electrons near this energy level. The highest splitting between the energy bands due to SOI is about 0.3 eV at high-symmetry points. Therefore, it is crucial to include SOI when calculating the MXene phase of  $\text{Ti}_3\text{C}_2(\text{OH})_2$ .

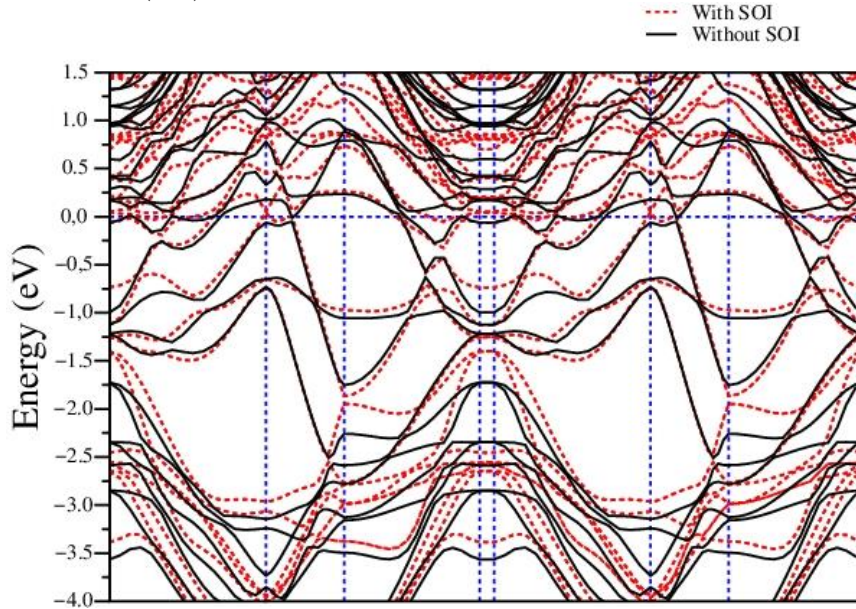


**Figure 6.** Electronic structures of  $\text{Ti}_3\text{C}_2(\text{OH})_2$  with (red dashed lines) and without (solid black lines) spin-orbit interactions

The high-symmetry points and Fermi surface (FS) sheets of the  $\text{Ti}_3\text{SiC}_2$  compound are presented in Figure 7, and are consistent with previous results [83]. Because SOI is not effective for this compound, the FS sheets with SOI are not shown in Figure 7. Six electronic bands crossed the  $E_F$ , forming six different FS. The first four FS had simple nesting around the  $\Gamma$  point. First, the FS enclosed the  $\Gamma$ -point in a spherical shape. The other three have a cylindrical shape, which also circles the  $\Gamma$  point. The fifth FS has more complex nesting than the first four FS. Although it rotates at the  $\Gamma$  point, it has a flower-like shape. The last FS has an enclosed shape around the K high-symmetry point. All the FS had both hole and electron pocket characteristics.

The FS sheets for  $\text{Ti}_3\text{C}_2(\text{OH})_2$  differ from the MAX phase owing to the effectiveness of the SOI. When the SOI is not considered, only two electronic bands cross the  $E_F$  and form two FS sheets, as shown in the left panel of Figure 8. The first one forms a flower-like nesting away from the zone center. The second has a similar shape away from the zone center, but also has two closed shapes around the  $\Gamma$  high-symmetry point.

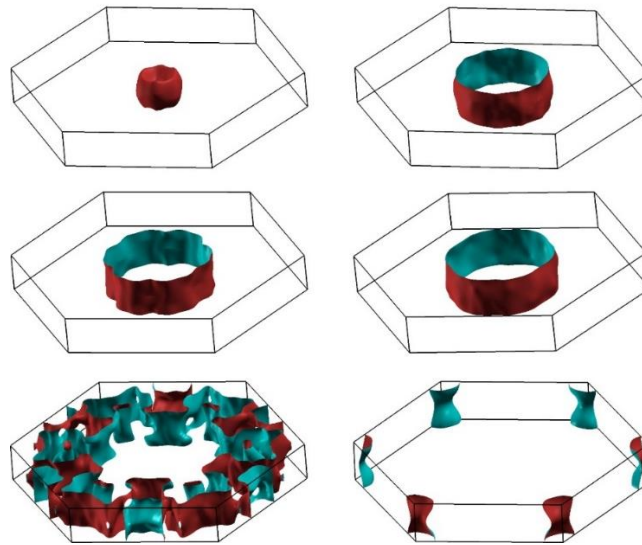


**Figure 7.** The Fermi Surface sheets for  $Ti_3SiC_2$  compound

The number of FS sheets increased when the SOI was included. The shape of the first FS does not change owing to the SOI, but the second one seems to be split into two different FS sheets that enhance the number of free electrons near the  $E_F$ . Nesting along the  $\Gamma - H$  direction can increase the scattering of electrons, which can increase the electron-phonon interaction. While the first FS with SOI had mainly hole-pocket features, the second and third FS sheets had electron-pocket features within the hexagonal MXene  $Ti_3C_2(OH)_2$ .

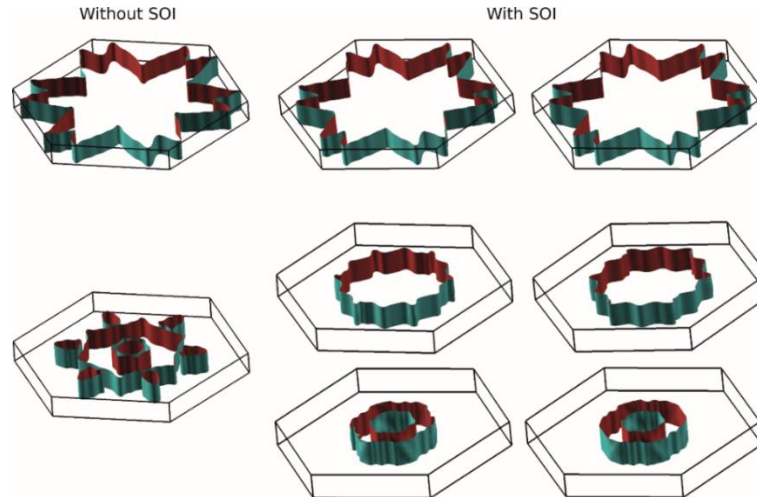


**Figure 8.** Fermi Surface sheets for  $Ti_3C_2(OH)_2$ . While the left column shows the sheets obtained without SOI, the middle and right columns correspond to the Fermi surface sheets obtained with SOI

The total and partial densities of state (DOS) of  $Ti_3SiC_2$  are shown in Figure 9. Because all atoms in the compound contribute to the DOS at the Fermi level ( $N(E_F)$ ), we can say that it exhibits a 3D-metallic electronic behavior. No gaps are observed in the valence bands of this compound. The  $N(E_F)$  value mainly consists of Ti 3d orbitals contributing to C 2p and Si 3p hybridization. The  $N(E_F)$  value for  $Ti_3SiC_2$  was calculated as 10.7 States/eV. The Ti 3d shell contributes approximately %65 (6.95 States/eV), the C 2p shell contributes around %17 (1.82 States/eV), and the Si 3p shell contributes to the  $N(E_F)$  around %15 (1.61 States/eV) of the  $Ti_3SiC_2$  compound. Although the d-orbital dominates the Fermi energy level, because the mass of the compound is relatively low, the SOI is not as effective as

that in a heavier mix. Hybridization occurred between the d- and p-orbitals in all energy regions. This hybridization is more distinctive in the valence region, suggesting solid bonding between Ti, C, and Si compounds. As the electronic structure implies, the SOI has a negligible effect on the electronic properties of this compound. Hence, only the DOS without the SOI is shown in Figure 9. The DOS and partial DOS features of  $\text{Ti}_3\text{C}_2(\text{OH})_2$  with and without SOI are shown in Figure 9. It can be seen that the multilayer structure is slightly disturbed after mixing with dimethylsulfoxide (Fig. 9).

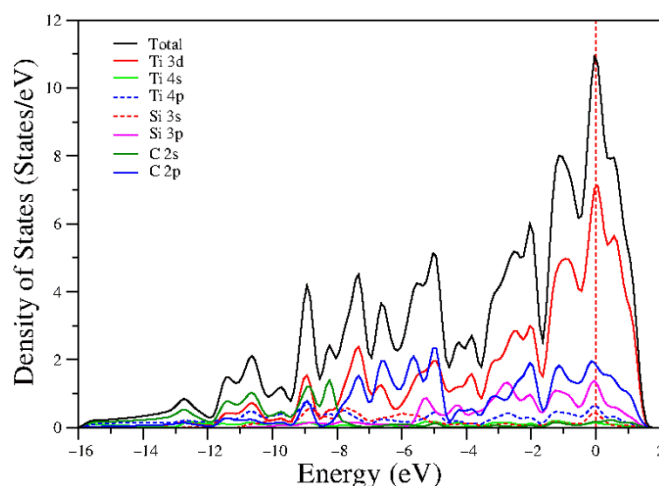


**Figure 9.** The total and partial density of states in  $\text{Ti}_3\text{SiC}_2$  orbitals

In Figure 10 (a), the DOS features of this compound are calculated using the SOI. Between -8.5 eV and -4.2 eV, O 2p shell makes the largest contribution the DOS features of the valence band. After this energy level to -2.5 eV, both Ti 3d and C 2p orbitals contribute equally to the DOS value. Near  $E_F$ , the Ti 3d shell dominated the electronic properties of  $\text{Ti}_3\text{C}_2(\text{OH})_2$ . A similar observation was made for the DOS properties calculated without an SOI, as shown in Figure 10 (b). The DOS features of  $\text{Ti}_3\text{C}_2(\text{OH})_2$  with and without SOI are shown in Figure 10. In Figure 10 (a), the DOS features of this compound were calculated using the SOI. Between -8.5 eV and -4.2 eV, the O 2p shell makes the most significant contribution to the DOS features of the valence band. After this energy level to -2.5 eV, the Ti 3d and C 2p orbitals contribute equally to the DOS value. Near  $E_F$ , the Ti 3d shell dominated the electronic properties of the  $\text{Ti}_3\text{C}_2(\text{OH})_2$  compound. A similar observation can be made for the DOS properties calculated without the SOI, as shown in Figure 10 (b). The main difference between these two graphs is the  $N(E_F)$  values. The  $N(E_F)$  value with SOI was calculated as 8.0 States/eV, whereas the corresponding value without SOI was obtained as 7.2 States/eV. This enhancement due to SOI can be explained by the gathering of split bands around  $E_F$ . The contribution of the Ti 3d shell to  $N(E_F)$  was approximately %74 with the SOI and %76 without the SOI. The C and O 2p orbitals contributed equally to  $N(E_F)$  in both calculations. We can say that even though the mass of the compound does not change significantly from the MAX phase to the MXene phase, because of the changing bonding features and contribution rates, SOI is much more effective in the MXene phase.

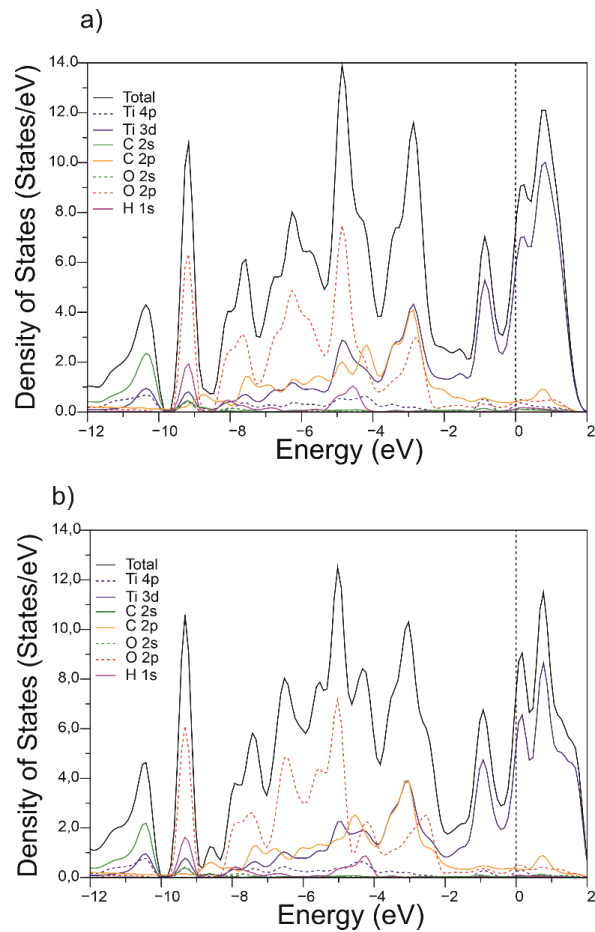


**Figure 10.** The density of states in  $\text{Ti}_3\text{C}_2(\text{OH})_2$  compounds (a) with and (b) without SOI

### 3. RESULTS AND DISCUSSION

The MAX phase starting powder broke the titanium-silicon bonds. Strong bonds existed between titanium and carbide, whereas weak bonds existed between titanium and silicon. In the  $\text{Ti}_3\text{C}_2\text{T}_x$  layers formed, MXenes exhibited weak Van der Waals bonds. The particles formed after hydrofluoric acid exfoliation were then exfoliated. Exfoliation results in an accordion-like shape [42], [52], [67]. The powders were coated with 80% gold and 20% palladium prior to SEM using Quorum Q150R ES brand coating equipment and a Polaron Range SC7620 Mini Sputter Coater. The researchers used a JEOL JSM-6060LV scanning electron microscope (SEM). Figure 11 shows SEM images of the  $\text{Ti}_3\text{SiC}_2$  MAX phase powder, which is referred to as the primary material.

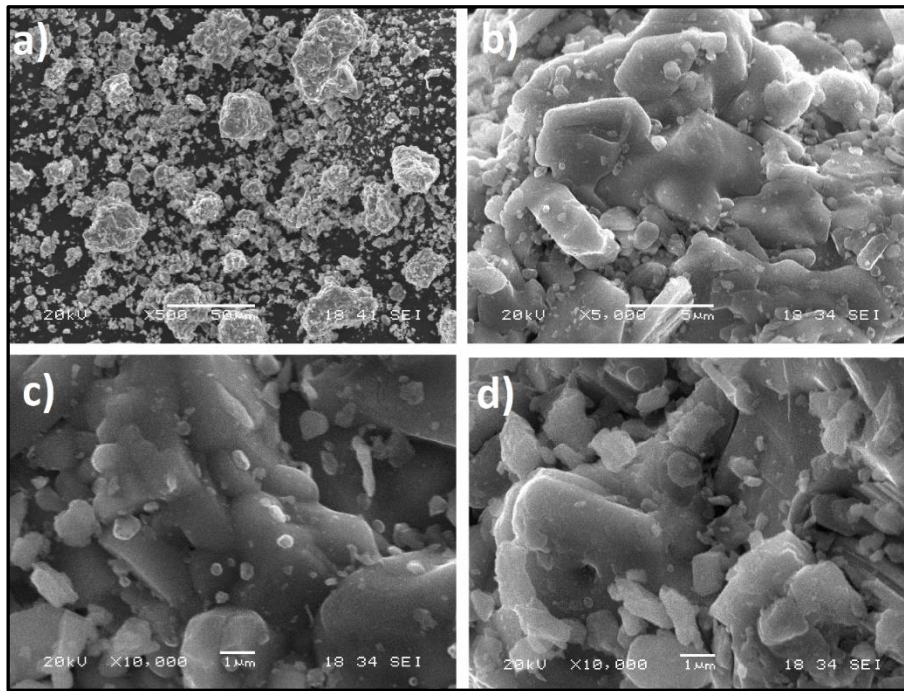


**Figure 11.** SEM images of  $Ti_3SiC_2$  MAX phase powder.

The samples were coded based on their operation. Hydrofluoric acid (HF) and dimethyl sulfoxide (DMSO) were used for coding. The mixing time with the acids was indicated by the sample code numbers (8 and 32 h). If treated with hydrofluoric acid, it is referred to as HF. It is classified as HF-HF if it has previously been treated with hydrofluoric acid and chemically treated with hydrofluoric acid. It was labelled with DMSO after treatment with acids and then combined with dimethyl sulfoxide. The powders were aggregated and the forms were more spherical, as shown in the SEM image of the basic material. The structures in which the stacked layers were best observed were the samples treated with a high mixing time, as shown by the SEM morphologies of the MXene powders (Figure 12).

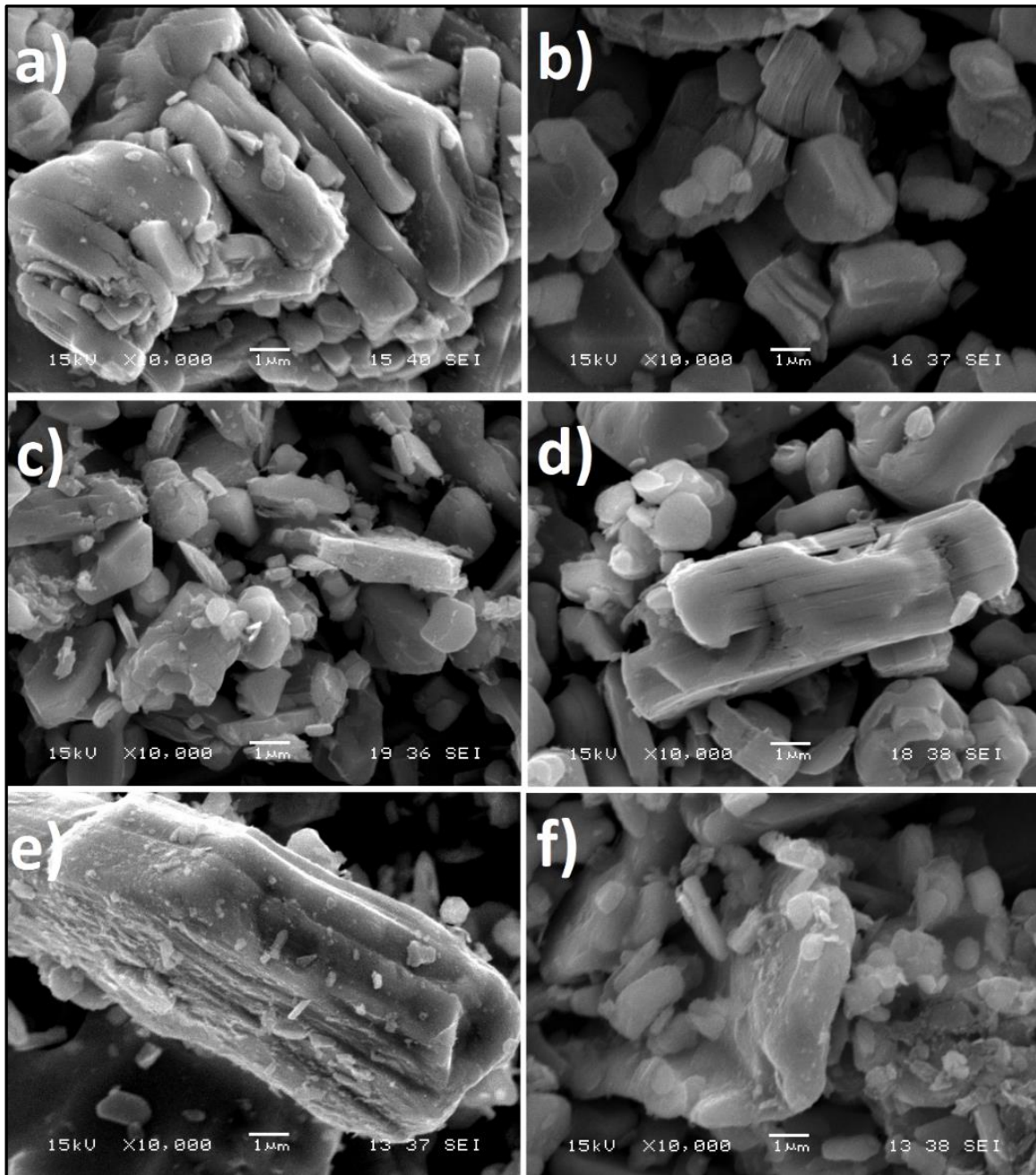


**Figure 12.** MXene structure ( $Ti_3C_2T_x$ ) powders a) HF-8, b) HF-32, c) HF-HF-8, d) HF-HF-32, e) HF-HF-DMSO-2, f) HF-HF-DMSO-32, SEM pictures

The powders acquired after 32 h of mixing were used to create SEM images, which clearly showed a layered structure (Figure 13). Field Emission Scanning Electron Microscopy (FE-SEM, FEI Quanta FEG 450) was used to characterize the materials. Figure 14 shows FE-SEM images of the MAX-phase  $Ti_3SiC_2$  sample used as the starting powder [63].

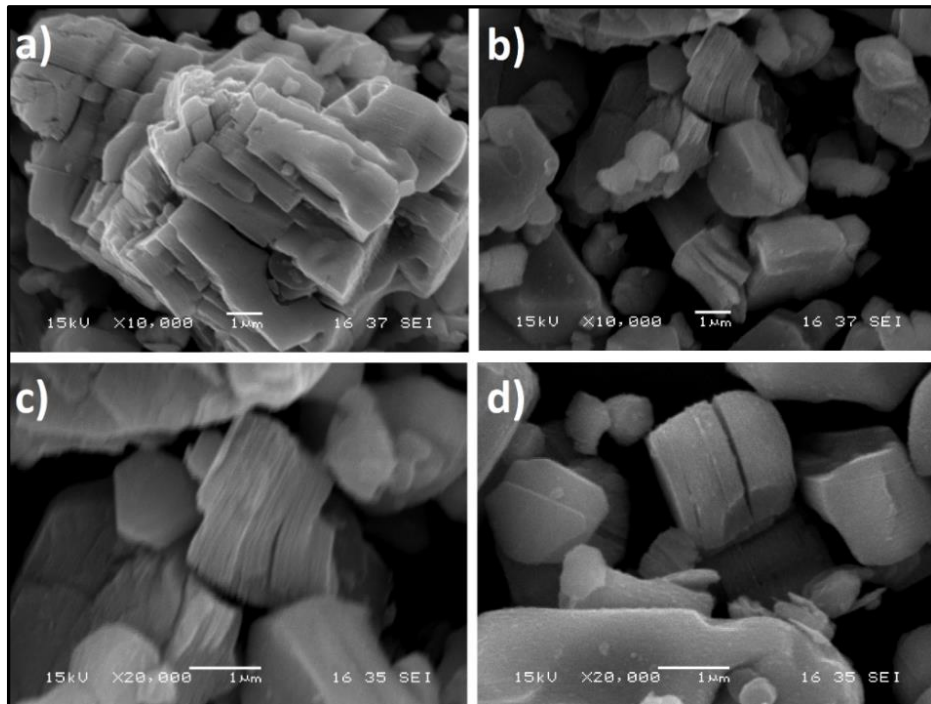


Figure 13. SEM images of HF-32 sample in MXene structure ( $Ti_3C_2T_x$ )

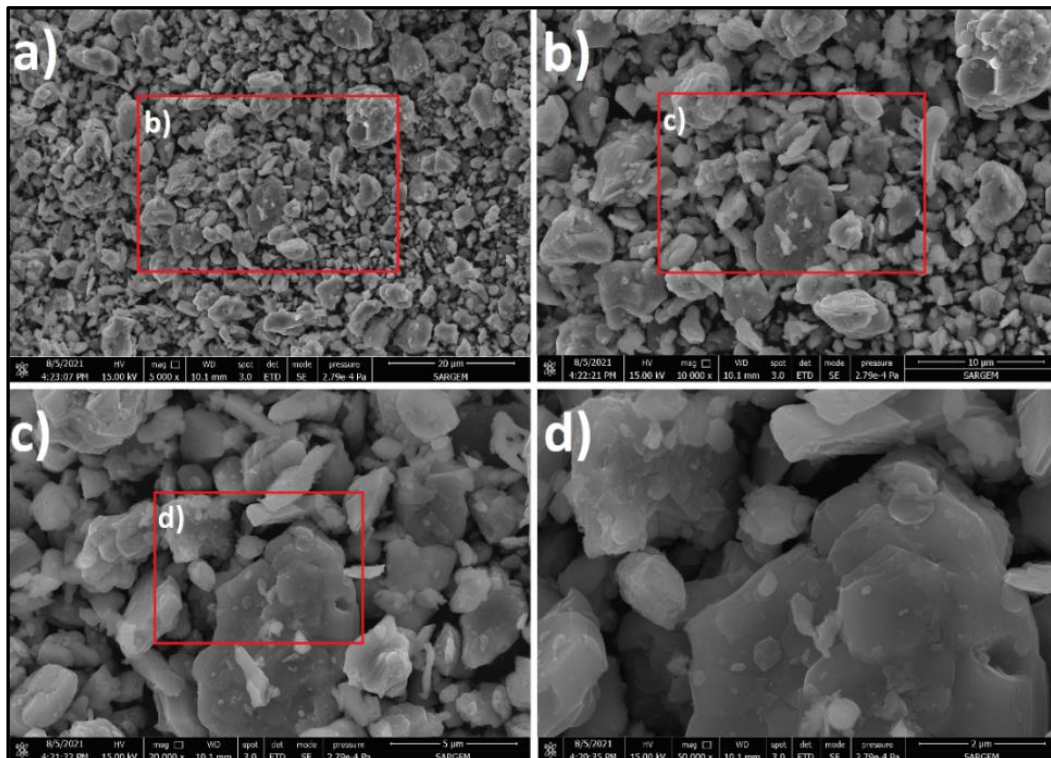


Figure 14. FE-SEM images of  $Ti_3SiC_2$  MAX phase powder.

Figure 15 shows FE-SEM EDX pictures of the MAX phase  $Ti_3SiC_2$  sample. According to the EDX images, the Ti content is approximately 70%. A layered structure was not observed in the initial powder.

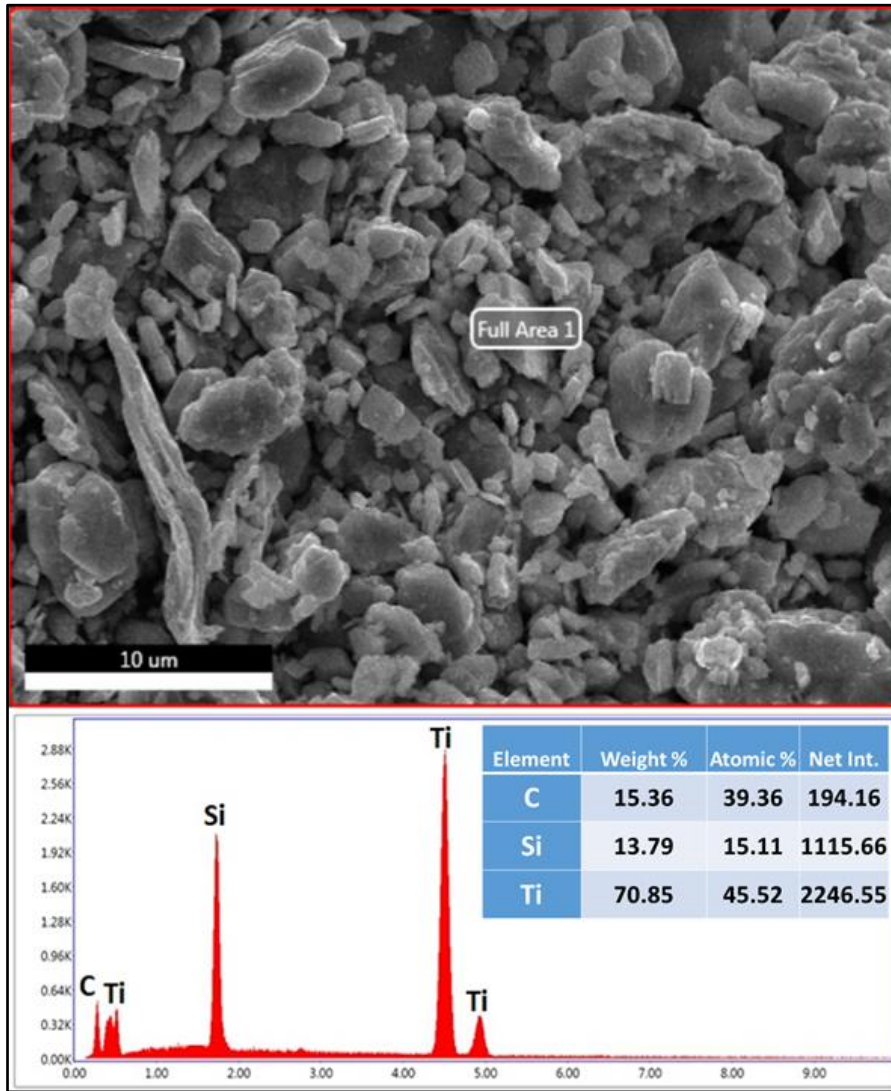
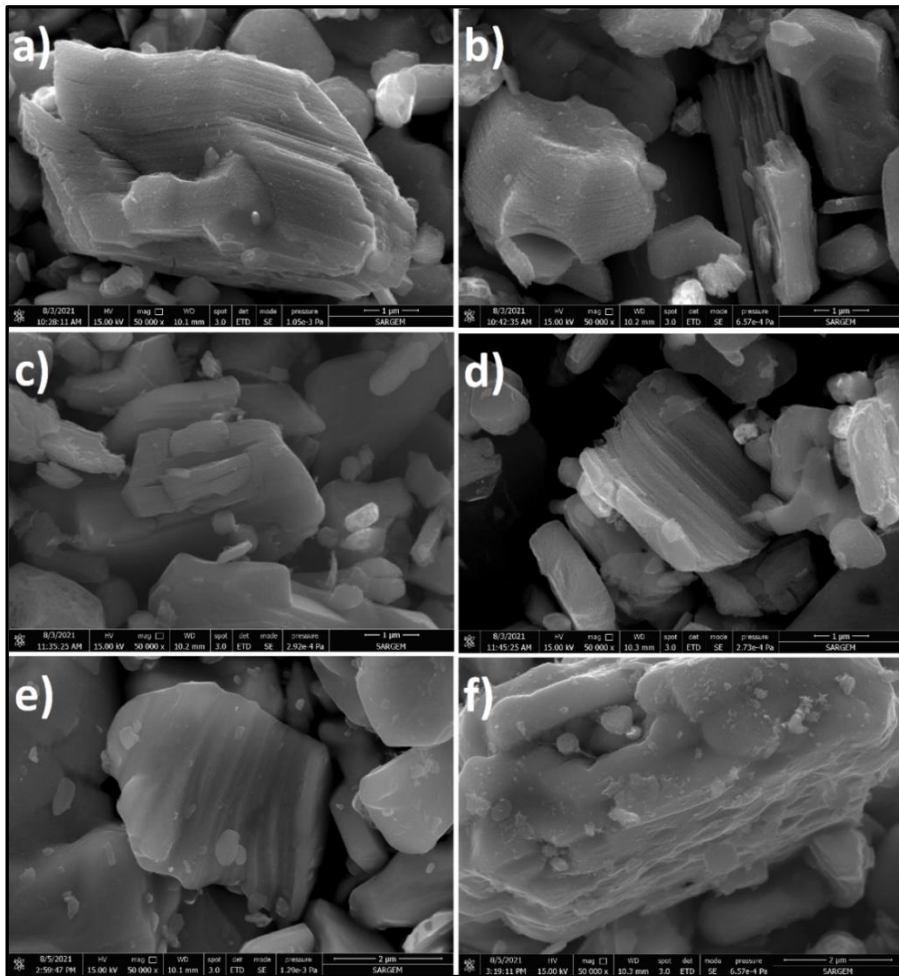
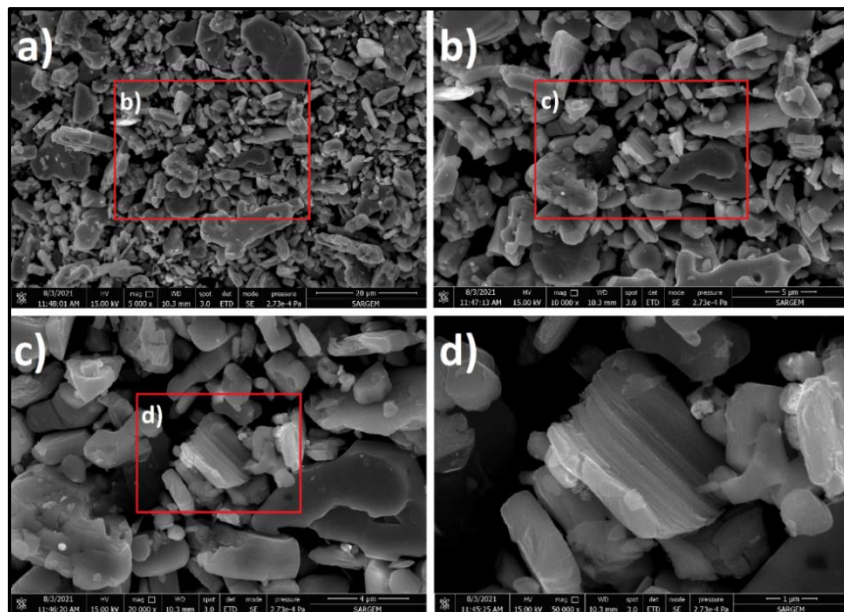


Figure 15. FE-SEM EDX images of  $Ti_3SiC_2$  MAX phase powder

Figure 16 shows the FE-SEM images of the samples prepared by mixing the MAX phase powder with hydrofluoric acid (HF) and then dimethyl sulfoxide (DMSO) for 8 and 32 h. The layered structures were formed after 32 h. At higher mixing speeds, the paper-like 2D structures, known as MXenes, became more dominant (Figure 17). Delamination is observed in the SEM and FE-SEM images as overlapping layers, which appear to have been sliced sharply with a metal blade [20]. The effect of the hydrofluoric acid mixing period was apparent in the HF-32 (Figure 16) [63] and HF-HF-32 (Figure 17) samples, where the layered structure was preserved, weak bonds were destroyed, and new layers were generated. The layered structures of HF-HF-DMSO-8 and HF-HF-DMSO-32 (Figure 16) with dimethyl sulfoxide were not entirely visible after mixing with hydrofluoric acid for 8 and 32 h, respectively.



**Figure 16.** Powders with MXene structure ( $Ti_3C_2T_x$ ) a) HF-8, b) HF-32, c) HF-HF-8, d) HF-HF-32, e) HF-HF-DMSO-8, and f) HF-HF-DMSO-32, FE-SEM images



**Figure 17.** FE-SEM images of HF-HF-32 sample

At four points selected from different locations in the SEM-EDX point analysis of the HF-HF-32 sample, there was a considerable drop in Si compared with the initial powder (Figure 18). Breaking Ti-Si bonds and eliminating Si from the environment are the main reasons for this.

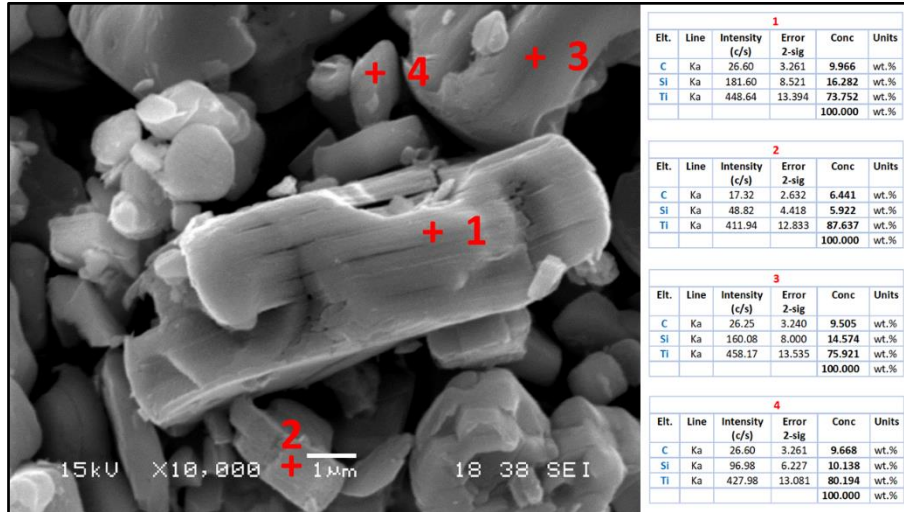


Figure 18. SEM EDX Spot Analysis of HF-HF-32 sample

Changes in Ti, Si, and C are visible in the SEM-EDX line analysis of the HF-HF-32 sample (Figure 19). The rate of silicon difference between the layers varied significantly. A linear relationship is observed between titanium and carbon. The elimination of Si from the environment due to reactions at specific locations is one of the most prominent reasons for this.

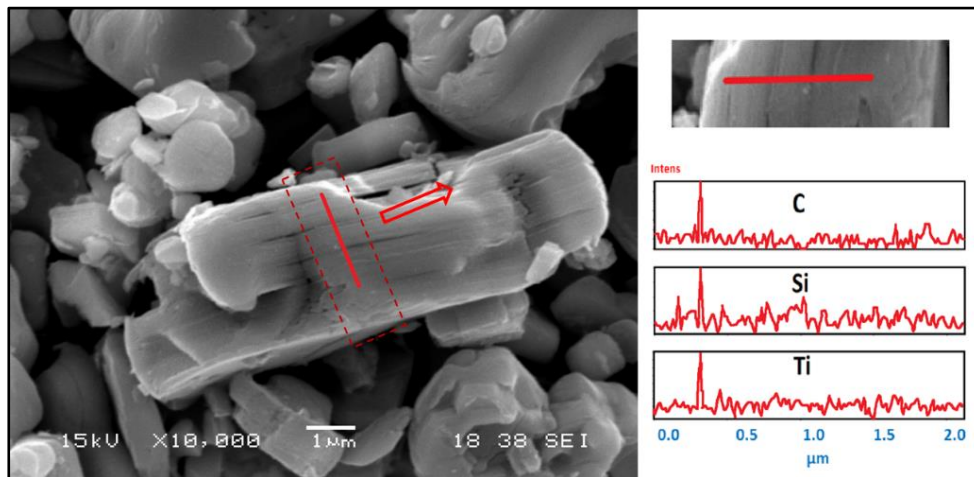


Figure 19. SEM EDX Line Analysis of HF-HF-32 sample

XRD analyses were performed using a RIGAKU D/MAX/2200/PC equipment and a Cu-supplied X-ray tube ( $\lambda = 1.54056$ ). The only MXene that has been successfully delaminated in substantial quantities is  $Ti_3C_2T_x$  [34]. XRD and EDS analyses confirmed the conversion of the MAX phase into MXene [8]. XRD studies of MAX-phase  $Ti_3SiC_2$  powder revealed similar characteristics [73]. Figure 20 shows XRD images of the MAX-phase  $Ti_3SiC_2$  sample used as the starting powder. The  $Ti_3SiC_2$  peak at  $39.779^\circ$  was the highest (104). The d value of this peak is  $2.2642 \text{ \AA}$  [63].

In general, XRD can identify intercalation because the interlayer spacing changes as a result of intercalation, which increases the c-lattice parameter (c-LP) and shifts the corresponding peak at two coordinates to the left [42]. The weakening or removal of all X-ray diffraction (XRD) peaks from the preceding MAX phase indicates effective etching from a crystallographic standpoint [15]. As the mixing temperature and duration were increased, d decreased. The XRD model will only have (0001) peaks (showing material loss in non-basal directions) if the MAX phase is completely converted to MXene, and all other heights will weaken or disappear. The (0001) elevations were initially broad and then narrowed as the angle decreased, suggesting that the lattice parameter increased [8]. The (002) and (004) peaks were split into two when the etching time was increased [1]. Figure 21 shows an XRD comparison of the MAX phase starting powder with MXene-based powders.

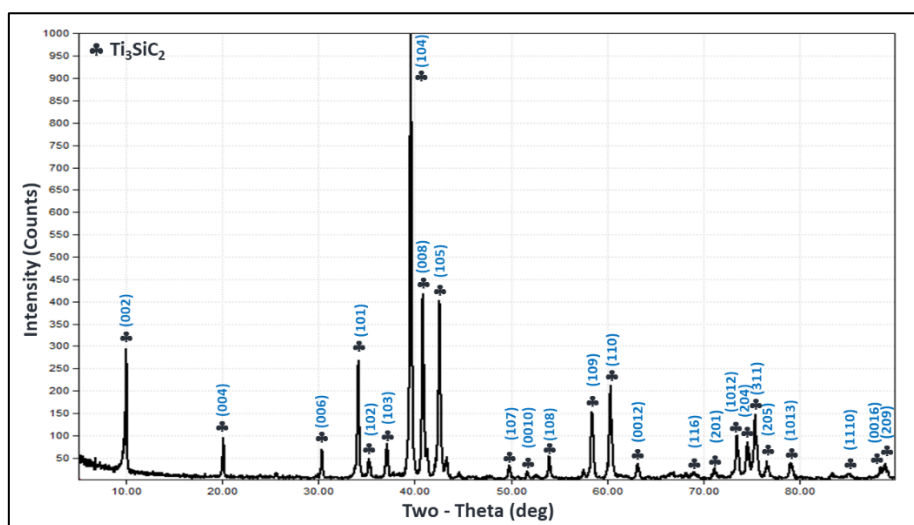


Figure 20. XRD Analysis of MAX phase  $Ti_3SiC_2$  sample

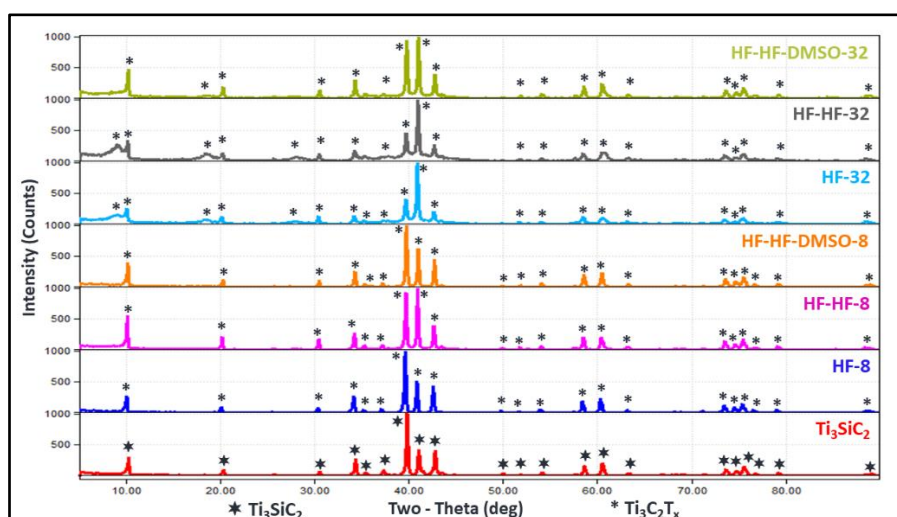


Figure 21. XRD analysis of MAX phase starting powder and other samples

The first (002) peak of the MAX phase shifted downward for  $Ti_3C_2T_x$  generated by direct HF exfoliation [13]. The (002), (004), and (006) planes of MXene are assigned to  $Ti_3C_2T_x$ . The (002) peak was considerably displaced in the spectra of the modified  $Ti_3C_2T_x$  and MXene. The high-order (004) and

(006) peaks behaved similarly. The lattice parameters of the modified samples illustrate the expansion of the c-plane distance [84]. (002), (004), (006), (008), and (009) are the XRD patterns of MXenes (110). With the addition of DMSO to MXene and sonication, the (002) pattern was exfoliated [64]. The peaks of the  $Ti_3SiC_2$  sample are displaced to the left by those of the hydrofluoric-acid-treated samples. Some of the peaks are smaller (Figure 22). The peaks at  $39.8^\circ$ ,  $41^\circ$ , and  $42.7^\circ$  showed an apparent shift. Compared to the initial powder, the peaks appeared to shift to the left.

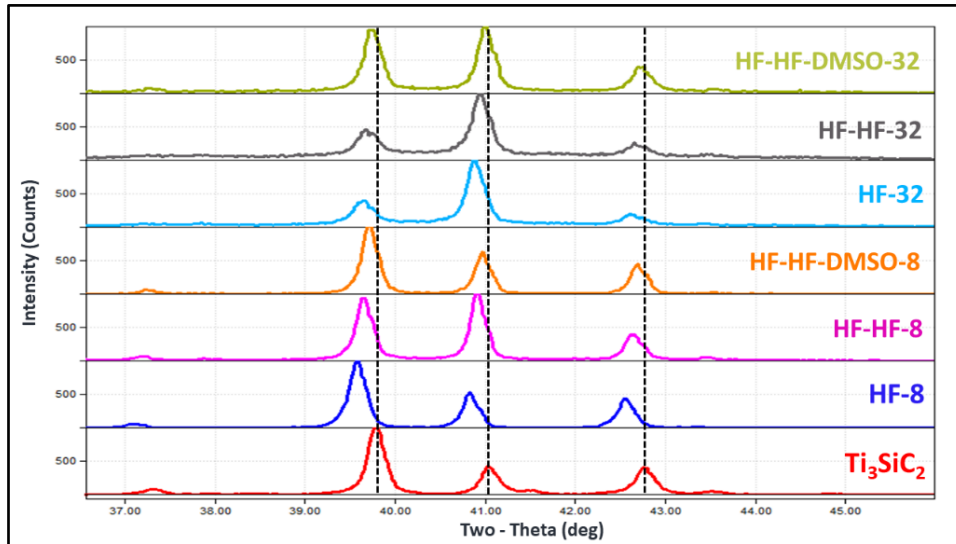


Figure 22. XRD analysis of MAX phase starting powder and other samples

After exfoliation, XRD analysis of the  $Ti_3C_2T_x$  sample revealed typical (0001) peaks, indicating that a layered structure was well formed. Dispersion and ultrasonication in ethanol and DMSO increased the intensity of the (002) peak [5]. Peaks (001), such as (002), (004), and (0010), on the other hand, expanded, lost intensity, and shifted to lower angles than their pre-processing positions [55]. MXene peaks are typically seen at  $9^\circ$  and  $19^\circ$  [1], [34], [78]. The XRD analysis of the HF-32 [63] and HF-HF-32 samples revealed MXene production (Figure 23).

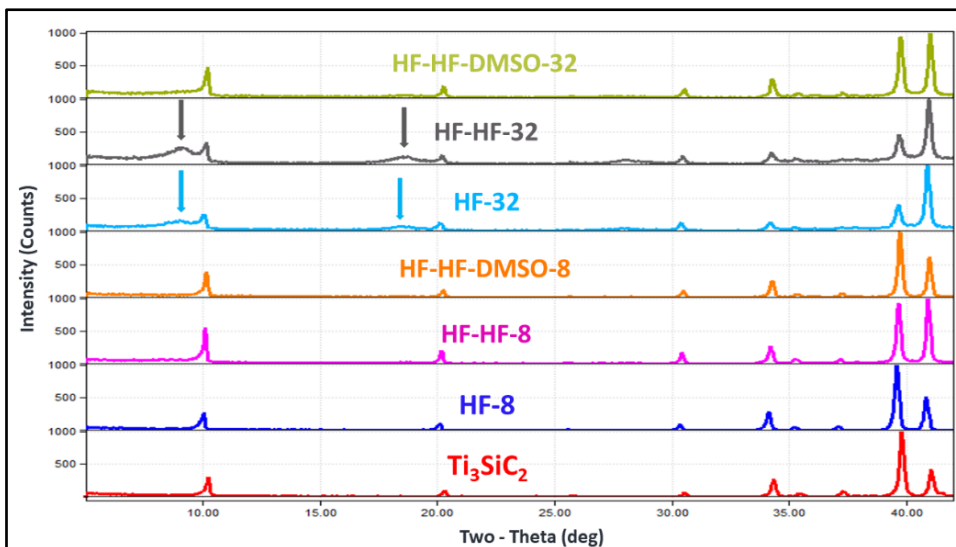


Figure 23. XRD analysis of Starting Powder and other samples

#### 4. CONCLUSIONS

The production of MXene is affected by the long mixing period with hydrofluoric acid. The Si concentration in the powder decreased after being treated twice with hydrofluoric acid. It is clear that MXene conversion occurred at high mixing speeds, resulting in silicon loss. An increase in the mixing time resulted in the formation of multilayer structures. Stratified structures did not form after 8 h of mixing. The inclusion of spin-orbit interaction in the theoretical calculations shows that even though the mass of the compound does not change significantly from the MAX phase to the MXene phase, because of the change in bonding features and density of states contribution rates, SOI is significantly more effective in the MXene phase. The effect of mixing time was observed in obtaining MXene. The structure formed after 32 h of mixing was more stable and two dimensional. This structure provides a positive change in the electronic properties. This is in agreement with the theoretical calculations. New generations of MXene materials are expected to be pioneers in electronic studies. Future studies on MXene compounds will focus on understanding the impact of various surface terminations and intercalations on the electronic, magnetic, and catalytic properties of these materials. . Research will continue to enhance the photocatalytic performance of  $Ti_3C_2(OH)_2$  for applications such as hydrogen production,  $CO_2$  reduction, and pollutant degradation. This includes the development of novel  $Ti_3C_2$ -based composites with materials like  $TiO_2$  to improve charge separation and photocatalytic efficiency.

#### Data Availability

The datasets used and/or analysed during the current study available from the corresponding author on reasonable request.

#### CONFLICT OF INTEREST

The author stated that there are no conflicts of interest regarding the publication of this article.

#### CRedit AUTHORSHIP CONTRIBUTION STATEMENT

**Mesut Ramazan Ekici:** Investigation, Methodology, Writing - original draft, Formal analysis, Writing - review & editing. **Hüseyin Yasin Uzunok:** Conceptualisation, Data curation, Methodology, Writing - review. **Emrah Bulut:** Writing, Supervision, Data Curation, Formal analysis. **Hüseyin Murat Tütüncü:** Writing, Formal analysis, Visualisation. **Ahmet Atasoy:** Writing, Supervision, Data Curation, Formal analysis.

#### REFERENCES

- [1] Su X, Zhang J, Mu H, et al. Effects of etching temperature and ball milling on the preparation and capacitance of  $Ti_3C_2$  MXene. *Journal of Alloys and Compounds*. 2018;752:32-39. doi:10.1016/j.jallcom.2018.04.152.
- [2] Zhu H. Functional metal carbide nano structures with unique thermal and electrical chemical properties. Published online 2018.
- [3] Shein IR, Ivanovskii AL. Graphene-like titanium carbides and nitrides  $Ti_{n+1}C_n$ ,  $Ti_{n+1}N_n$  ( $n = 1, 2,$  and 3) from de-intercalated MAX phases: First-principles probing of their structural, electronic properties and relative stability. *Computational Materials Science*. 2012;65:104-114. doi:10.1016/j.commatsci.2012.07.011.
- [4] Agartan L, Hantanasirisakul K, Buczek S, et al. Influence of operating conditions on the

- desalination performance of a symmetric pre-conditioned  $Ti_3C_2T_x$ -MXene membrane capacitive deionization system. *Desalination*. 2020;477. doi:10.1016/j.desal.2019.114267.
- [5] Lv G, Wang J, Shi Z, Fan L. Intercalation and delamination of two-dimensional MXene ( $Ti_3C_2T_x$ ) and application in sodium-ion batteries. *Materials Letters*. 2018;219:45-50. doi:10.1016/j.matlet.2018.02.016.
- [6] Salim O, Mahmoud KA, Pant KK, Joshi RK. Introduction to MXenes: synthesis and characteristics. *Materials Today Chemistry*. 2019;14:100191. doi:10.1016/j.mtchem.2019.08.010.
- [7] Eklund P, Rosen J, Persson POÅ. Layered ternary  $M_{n+1}AX_n$  phases and their 2D derivative MXene: An overview from a thin-film perspective. *Journal of Physics D: Applied Physics*. 2017;50(11). doi:10.1088/1361-6463/aa57bc.
- [8] Venkateshalu S, Grace AN. MXenes-A new class of 2D layered materials: Synthesis, properties, applications as supercapacitor electrode and beyond. *Applied Materials Today*. 2020;18:100509. doi:10.1016/j.apmt.2019.100509.
- [9] Alhabe M, Maleski K, Mathis TS, et al. Selective Etching of Silicon from  $Ti_3SiC_2$  (MAX) To Obtain 2D Titanium Carbide (MXene). *Angewandte Chemie - International Edition*. 2018;57(19):5444-5448. doi:10.1002/anie.201802232.
- [10] Cui G, Zheng X, Lv X, Jia Q, Xie W, Gu G. Synthesis and microwave absorption of  $Ti_3C_2T_x$  MXene with diverse reactant concentration, reaction time, and reaction temperature. *Ceramics International*. 2019;45(17):23600-23610. doi:10.1016/j.ceramint.2019.08.071.
- [11] Gogotsi Y, Anasori B. The Rise of MXenes. *ACS Nano*. 2019;13(8):8491-8494. doi:10.1021/acsnano.9b06394.
- [12] Zhao S, Nivetha R, Qiu Y, Guo X. Two-dimensional hybrid nanomaterials derived from MXenes ( $Ti_3C_2T_x$ ) as advanced energy storage and conversion applications. *Chinese Chemical Letters*. 2020;31(4):947-952. doi:10.1016/j.cclet.2019.11.045.
- [13] Rasool K, Pandey RP, Rasheed PA, Buczek S, Gogotsi Y, Mahmoud KA. Water treatment and environmental remediation applications of two-dimensional metal carbides (MXenes). *Materials Today*. 2019;30(November):80-102. doi:10.1016/j.mattod.2019.05.017.
- [14] Halim J, Cook KM, Naguib M, et al. X-ray photoelectron spectroscopy of select multi-layered transition metal carbides (MXenes). *Applied Surface Science*. 2016;362:406-417. doi:10.1016/j.apsusc.2015.11.089.
- [15] Collini P. Deposizione Elettroforetica Di Film Di Mxene Per Applicazioni Funzionali. *MaxMaterialsDrexelEdu*. Published online 2017. [http://max.materials.drexel.edu/wp-content/uploads/Pieralberto\\_Collini.pdf](http://max.materials.drexel.edu/wp-content/uploads/Pieralberto_Collini.pdf).
- [16] Tang J, Yi W, Zhong X, et al. Laser writing of the restacked titanium carbide MXene for high performance supercapacitors. *Energy Storage Materials*. 2020;32(July):418-424. doi:10.1016/j.ensm.2020.07.028.
- [17] Wild M, Gregory J. *Offe. Lithium-Sulfur Batteries*. John Wiley & Sons Ltd; 2019.

- [18] Shi L. From MAX phases to MXenes : synthesis, characterization and electronic properties. Published online 2017.
- [19] Jo G. Proton Hopping in a Single Layer Water Between MXene Layers Using ReaxFF MD Simulation. 2017;(May).
- [20] Halim J. Synthesis and Characterization of 2D Nanocrystals and Thin Films of Transition Metal Carbides (MXenes). 2014;(1679). doi:10.3384/lic.diva-111128.
- [21] Magné D. Synthèse et structure électronique de phases MAX et MXènes. Published online 2016. <http://nuxeo.edel.univ-poitiers.fr/nuxeo/site/esupversions/83ffbfba-e881-4604-9aff-2875945e1f3b>.
- [22] M. Higashi, S. Momono, K. Kishida, N. L. Okamoto, and H. Inui, “Anisotropic plastic deformation of single crystals of the MAX phase compound  $Ti_3SiC_2$  investigated by micropillar compression,” *Acta Materialia*, vol. 161, pp. 161–170, 2018, doi: 10.1016/j.actamat.2018.09.024.
- [23] Zhu M, Wang R, Chen C, Zhang HB, Zhang GJ. Comparison of corrosion behavior of  $Ti_3SiC_2$  and  $Ti_3AlC_2$  in NaCl solutions with Ti. *Ceramics International*. 2017;43(7):5708-5714. doi:10.1016/j.ceramint.2017.01.111.
- [24] Sun ZM, Zou Y, Tada S, Hashimoto H. Effect of Al addition on pressureless reactive sintering of  $Ti_3SiC_2$ . *Scripta Materialia*. 2006;55(11):1011-1014. doi:10.1016/j.scriptamat.2006.08.019.
- [25] Zhang J, Wang L, Jiang W, Chen L. Effect of TiC content on the microstructure and properties of  $Ti_3SiC_2$ -TiC composites in situ fabricated by spark plasma sintering. *Materials Science and Engineering A*. 2008;487(1-2):137-143. doi:10.1016/j.msea.2007.12.004.
- [26] Anasori B, Lukatskaya MR, Gogotsi Y. 2D metal carbides and nitrides (MXenes) for energy storage. *Nature Reviews Materials*. 2017;2(2). doi:10.1038/natrevmats.2016.98.
- [27] Li J, Kurra N, Seredych M, Meng X, Wang H, Gogotsi Y. Bipolar carbide-carbon high voltage aqueous lithium-ion capacitors. *Nano Energy*. 2019;56(November 2018):151-159. doi:10.1016/j.nanoen.2018.11.042.
- [28] Hu T, Yang J, Wang X. Carbon vacancies in  $Ti_2CT_2$  MXenes: Defects or a new opportunity? *Physical Chemistry Chemical Physics*. 2017;19(47):31773-31780. doi:10.1039/c7cp06593k.
- [29] Wang Y, Feng W, Chen Y. Chemistry of two-dimensional MXene nanosheets in theranostic nanomedicine. *Chinese Chemical Letters*. 2020;31(4):937-946. doi:10.1016/j.ccllet.2019.11.016.
- [30] Ward J, Middleburgh S, Topping M, et al. Crystallographic evolution of MAX phases in proton irradiating environments. *Journal of Nuclear Materials*. 2018;502:220-227. doi:10.1016/j.jnucmat.2018.02.008.
- [31] Jung Y II, Park DJ, Park JH, Park JY, Kim HG, Koo YH. Effect of  $TiSi_2/Ti_3SiC_2$  matrix phases in a reaction-bonded SiC on mechanical and high-temperature oxidation properties. *Journal of the European Ceramic Society*. 2016;36(6):1343-1348. doi:10.1016/j.jeurceramsoc.2016.01.015.
- [32] Khazaei M, Ranjbar A, Arai M, Sasaki T, Yunoki S. Electronic properties and applications of MXenes: a theoretical review. *Journal of Materials Chemistry C*. 2017;5(10):2488-2503. doi:10.1039/c7tc00140a.

- [33] Acerce M. Electrochemical Charge Storage and Electrochemomechanical Behavior of Chemically Exfoliated & Restacked MoS<sub>2</sub> Nanosheets. Published online 2016.
- [34] Abdelmalak MN. MXenes: A New Family of Two-Dimensional Materials and its Application as Electrodes for Li-ion Batteries. Published online 2014.
- [35] Boota M. Redox-Active Hybrid Materials for Pseudocapacitive Energy Storage. ECS Meeting Abstracts. 2017;(September). doi:10.1149/ma2017-01/43/2013.
- [36] Ghidui MJ. Ions in MXene: Characterization and Control of Interlayer Cations and their Effects on Structure and Properties of 2D Transition Metal Carbides. 2018;(June).
- [37] Colón MG. Max-Phase Slurry Coatings For High Temperature Oxidation Protection of Ti Based Alloys. Published online 2014.
- [38] Lane NJ. Lattice Dynamical Studies of Select MAX Phases. 2013;(April).
- [39] Karlsson L. Transmission Electron Microscopy of 2D Materials: Structure and Surface Properties. 2016;(1745). doi:10.3384/diss.diva-127526.
- [40] Zhang X, Liu Y, Dong S, Yang J, Liu X. Flexible electrode based on multi-scaled MXene (Ti<sub>3</sub>C<sub>2</sub>T<sub>x</sub>) for supercapacitors. Journal of Alloys and Compounds. 2019;790:517-523. doi:10.1016/j.jallcom.2019.03.219.
- [41] Wen Y, Rufford TE, Chen X, et al. Nitrogen-doped Ti<sub>3</sub>C<sub>2</sub>T<sub>x</sub> MXene electrodes for high-performance supercapacitors. Nano Energy. 2017;38(June):368-376. doi:10.1016/j.nanoen.2017.06.009.
- [42] Lukatskaya MR. Capacitive Performance of Two-Dimensional Metal Carbides. 2015;(December). doi:10.1145/3132847.3132886.
- [43] Ahmed B. Surface Modification of MXenes: A Pathway to Improve MXene Electrode Performance in Electrochemical Energy Storage Devices. Published online 2017.
- [44] Rajagopalan Kannan DR, Terala PK, Moss PL, Weatherspoon MH. Analysis of the Separator Thickness and Porosity on the Performance of Lithium-Ion Batteries. International Journal of Electrochemistry. 2018;2018:1-7. doi:10.1155/2018/1925708.
- [45] Meng J, Zhang F, Zhang L, et al. Rolling up MXene sheets into scrolls to promote their anode performance in lithium-ion batteries. Journal of Energy Chemistry. 2020;46:256-263. doi:10.1016/j.jechem.2019.10.008.
- [46] Wang CH, Kurra N, Alhabeb M, Chang JK, Alshareef HN, Gogotsi Y. Titanium Carbide (MXene) as a Current Collector for Lithium-Ion Batteries. ACS Omega. 2018;3(10):12489-12494. doi:10.1021/acsomega.8b02032.
- [47] Tang H, Li W, Pan L, et al. A Robust, Freestanding MXene-Sulfur Conductive Paper for Long-Lifetime Li-S Batteries. Advanced Functional Materials. 2019;29(30):1-10. doi:10.1002/adfm.201901907.
- [48] Jiang W, Henager CH, Varga T, et al. Diffusion of Ag, Au and Cs implants in MAX phase

- Ti<sub>3</sub>SiC<sub>2</sub>. Journal of Nuclear Materials. 2015;462:310-320. doi:10.1016/j.jnucmat.2015.04.002
- [49] Jacques S, Fakih H, Viala JC. Reactive chemical vapor deposition of Ti<sub>3</sub>SiC<sub>2</sub> with and without pressure pulses: Effect on the ternary carbide texture. Thin Solid Films. 2010;518(18):5071-5077. doi:10.1016/j.tsf.2010.02.059.
- [50] Cao MS, Cai YZ, He P, Shu JC, Cao WQ, Yuan J. 2D MXenes: Electromagnetic property for microwave absorption and electromagnetic interference shielding. Chemical Engineering Journal. 2019;359(November 2018):1265-1302. doi:10.1016/j.cej.2018.11.051.
- [51] Min B. Broadly defined synthesis and properties of phase change materials. Published online 2018.
- [52] Mashtalir O. Chemistry of Two-Dimensional Transition Metal Carbides (MXenes). Published online 2015.
- [53] Jaffari ZH, Abuabdou SMA, Ng D-Q, Bashir MJK. Insight into two-dimensional MXenes for environmental applications: Recent progress, challenges, and prospects. FlatChem. 2021;28(April):100256. doi:10.1016/j.flatc.2021.100256.
- [54] Ashton M. Computational Methods for the Discovery and Characterization of Two-Dimensional Materials. Published online 2017.
- [55] Naguib M, Kurtoglu M, Presser V, et al. Two-Dimensional Nanocrystals Produced by Exfoliation of Ti<sub>3</sub>AlC<sub>2</sub>. Advanced Materials. 2011;23(37):4248-4253. doi:10.1002/adma.201102306.
- [56] Liao Y, Qian J, Xie G, et al. 2D-layered Ti<sub>3</sub>C<sub>2</sub> MXenes for promoted synthesis of NH<sub>3</sub> on P<sub>25</sub> photocatalysts. Applied Catalysis B: Environmental. 2020;273(February):119054. doi:10.1016/j.apcatb.2020.119054.
- [57] Wen Y, Li R, Liu J, et al. A temperature-dependent phosphorus doping on Ti<sub>3</sub>C<sub>2</sub>T<sub>x</sub> MXene for enhanced supercapacitance. Journal of Colloid and Interface Science. 2021;604:239-247. doi:10.1016/j.jcis.2021.06.020.
- [58] Chen Y-H, Qi M-Y, Li Y-H, et al. Activating two-dimensional Ti<sub>3</sub>C<sub>2</sub>T<sub>x</sub>-MXene with single-atom cobalt for efficient CO<sub>2</sub> photoreduction. Cell Reports Physical Science. 2021;2(3):100371. doi:10.1016/j.xcrp.2021.100371.
- [59] Zhao X, Chen J, Zhao C, et al. Construction ZnIn<sub>2</sub>S<sub>4</sub>/Ti<sub>3</sub>C<sub>2</sub> of 2D/2D heterostructures with enhanced visible light photocatalytic activity: A combined experimental and first-principles DFT study. Applied Surface Science. 2021;570(August):151183. doi:10.1016/j.apsusc.2021.151183.
- [60] Mondal K, Ghosh P. Exfoliation of Ti<sub>2</sub>C and Ti<sub>3</sub>C<sub>2</sub> Mxenes from bulk trigonal phases of titanium carbide: A theoretical prediction. Solid State Communications. 2019;299(March):113657. doi:10.1016/j.ssc.2019.113657.
- [61] Ekici MR, Atasoy A. Graphene Alternative 2D Materials: MXene. In: 20th International Metallurgy and Materials Congress. ; 2021:396-400.
- [62] Ekici MR, Atasoy A. Effect of HF Acid on The Formation of New 2D Ti<sub>3</sub>C<sub>2</sub> Mxene From Ti<sub>3</sub>SiC<sub>2</sub>. Selcuk University Journal of Engineering Sciences. 2020;Special Is(1):1-23. <https://sujes.selcuk.edu.tr/sujes/article/view/512>.

- [63] Ekici MR, Tabar E, Atasoy A, Bulut E, Hoşgör G. Effect of hydrochloric acid and hydrofluoric acid treatment on the morphology, structure and gamma permeability of 2D MXene  $Ti_3C_2T_x$  electrodes. *Canadian Metallurgical Quarterly*. Published online September 16, 2022:1-22. doi:10.1080/00084433.2022.2124108.
- [64] Chae A, Jang H, Koh DY, Yang CM, Kim YK. Exfoliated MXene as a mediator for efficient laser desorption/ionization mass spectrometry analysis of various analytes. *Talanta*. 2020;209(November 2019):120531. doi:10.1016/j.talanta.2019.120531.
- [65] Ren C (Evelyn). Interaction of Ions with Two-Dimensional Transition Metal Carbide (MXene) Films. ProQuest Dissertations and Theses. 2017;(July).
- [66] Dall’Agnese Y. Study of Early Transition Metal Carbides for Energy Storage Applications. 2016;(March).
- [67] Steinberg J a. Formation of Thin Films from MXene Flakes. Published online 2013.
- [68] Zhang C (John), Nicolosi V. Graphene and MXene-based transparent conductive electrodes and supercapacitors. *Energy Storage Materials*. 2019;16(May 2018):102-125. doi:10.1016/j.ensm.2018.05.003.
- [69] Shah JB. Synthesis of MXene-Epoxy Nanocomposites. 2017;(June).
- [70] Hatter CB, Shah J, Anasori B, Gogotsi Y. Micromechanical response of two-dimensional transition metal carbonitride (MXene) reinforced epoxy composites. *Composites Part B: Engineering*. 2020;182(June 2019):107603. doi:10.1016/j.compositesb.2019.107603.
- [71] Rosenkranz A, Grützmacher PG, Espinoza R, et al. Multi-layer  $Ti_3C_2T_x$ -nanoparticles (MXenes) as solid lubricants - Role of surface terminations and intercalated water. *Applied Surface Science*. 2019;494(July):13-21. doi:10.1016/j.apsusc.2019.07.171.
- [72] Zhang S. Study of chemical reactivity of MAX phase single crystals. Published online 2018.
- [73] Aghamohammadi H, Heidarpour A, Jamshidi R. The phase and morphological evolution of  $Ti_3SiC_2$  MAX phase powder after HF treatment. *Ceramics International*. 2018;44(15):17992-18000. doi:10.1016/j.ceramint.2018.06.278.
- [74] Piechowiak MA, Henon J, Durand-Panteix O, et al. Growth of dense  $Ti_3SiC_2$  MAX phase films elaborated at room temperature by aerosol deposition method. *Journal of the European Ceramic Society*. 2014;34(5):1063-1072. doi:10.1016/j.jeurceramsoc.2013.11.019.
- [75] Schultheiß J, Dermeik B, Filbert-Demut I, et al. Processing and characterization of paper-derived  $Ti_3SiC_2$  based ceramic. *Ceramics International*. 2015;41(10):12595-12603. doi:10.1016/j.ceramint.2015.06.085.
- [76] Guo J, Zhao Y, Liu A, Ma T. Electrostatic self-assembly of 2D delaminated MXene ( $Ti_3C_2$ ) onto Ni foam with superior electrochemical performance for supercapacitor. *Electrochimica Acta*. 2019;305:164-174. doi:10.1016/j.electacta.2019.03.025.
- [77] Rangom YP. Double Layer Formation and Cation Pseudo- Intercalation Supercapacitor Carbon Nanotube Composite Electrodes with Enhanced Electrochemical Performances. Published online

2014.

- [78] Li Z, Wang L, Sun D, et al. Synthesis and thermal stability of two-dimensional carbide MXene  $Ti_3C_2$ . *Materials Science and Engineering B: Solid-State Materials for Advanced Technology*. 2015;191(C):33-40. doi:10.1016/j.mseb.2014.10.009.
- [79] Giannozzi P, Baroni S, Bonini N, et al. QUANTUM ESPRESSO: a Modular and Open-source Software project for Quantum Simulations of Materials. *Journal of Physics: Condensed Matter*. 2009;21(39):395502. doi:10.1088/0953-8984/21/39/395502.
- [80] Giannozzi P, Andreussi O, Brumme T, et al. Advanced Capabilities for Materials Modelling With Quantum ESPRESSO. *Journal of Physics: Condensed Matter*. 2017;29(46):465901. doi:10.1088/1361-648X/aa8f79.
- [81] Perdew JP, Burke K, Ernzerhof M. Generalized Gradient Approximation Made Simple. *Physical Review Letters*. 1996;77(18):3865-3868. doi:10.1103/PhysRevLett.77.3865.
- [82] Arunajatesan S, Carim AH. Symmetry and crystal structure of  $Ti_3SiC_2$ . *Materials Letters*. 1994;20(5-6):319-324. doi:10.1016/0167-577X(94)90037-X.
- [83] Pinek D, Ito T, Furuta K, et al. Near Fermi Level Electronic Structure of  $Ti_3SiC_2$  Revealed by Angle-resolved Photoemission Spectroscopy. *Physical Review B*. 2020;102(7):075111. doi:10.1103/PhysRevB.102.075111.
- [84] Zhang L, Su W, Shu H, et al. Tuning the photoluminescence of large  $Ti_3C_2T_x$  MXene flakes. *Ceramics International*. 2019;45(9):11468-11474. doi:10.1016/j.ceramint.2019.03.014.